

DA-VPT: Semantic-Guided Visual Prompt Tuning for Vision Transformers

Li Ren, Chen Chen, Liqiang Wang, Kien Hua

Department of Computer Science
University of Central Florida, USA

{Li.Ren, Chen.Chen, Liqiang.Wang, Kien.Hua}@ucf.edu

Abstract

Visual Prompt Tuning (VPT) has become a promising solution for Parameter-Efficient Fine-Tuning (PEFT) approach for Vision Transformer (ViT) models by partially fine-tuning learnable tokens while keeping most model parameters frozen. Recent research has explored modifying the connection structures of the prompts. However, the fundamental correlation and distribution between the prompts and image tokens remain unexplored. In this paper, we leverage metric learning techniques to investigate how the distribution of prompts affects fine-tuning performance. Specifically, we propose a novel framework, **Distribution Aware Visual Prompt Tuning (DA-VPT)**, to guide the distributions of the prompts by learning the distance metric from their class-related semantic data. Our method demonstrates that the prompts can serve as an effective bridge to share semantic information between image patches and the class token. We extensively evaluated our approach on popular benchmarks in both recognition and segmentation tasks. The results demonstrate that our approach enables more effective and efficient fine-tuning of ViT models by leveraging semantic information to guide the learning of the prompts, leading to improved performance on various downstream vision tasks. The code is released on <https://github.com/Noahsark/DA-VPT>.

1. Introduction

Recent advances in model scaling and dataset expansion [13, 50, 69] have led to powerful vision foundation models, particularly those based on Vision Transformer (ViT) architectures [14]. These models have demonstrated exceptional performance across various computer vision tasks [26, 27, 63]. While fine-tuning these models for downstream tasks like visual recognition [14] or semantic segmentation [37] has become standard practice, the conventional full fine-tuning approach faces significant challenges, including high computational costs, overfitting, and catastrophic forgetting [38, 55]. These challenges have motivated the development

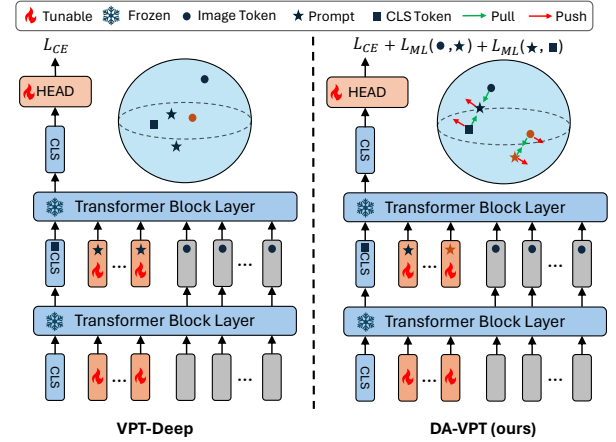


Figure 1. **Comparison between VPT-Deep and DA-VPT.** **Left (VPT-Deep):** Prompts are guided solely by the recognition task, leading to unconstrained distributions between prompts and visual tokens. This allows prompts to attract features from arbitrary classes, potentially hindering the class token’s ability to aggregate class-specific information. **Right (DA-VPT):** Prompts are jointly optimized by the main task and semantic metric learning objectives. The semantic clustering aligns the distributions of prompts, visual tokens, and class tokens, enabling more effective class-specific information aggregation through semantically-guided attention.

of Parameter-Efficient Fine-Tuning (PEFT) methods that selectively update a small subset of model parameters while keeping the majority frozen [4, 31, 33, 38, 44, 61, 66, 86].

Initially emerging from the NLP domain, Houlsby et al. [31] and subsequent works [32, 61] demonstrated that updating a minimal number of parameters could achieve performance comparable to full fine-tuning. These techniques were later adapted to computer vision by Chen et al. [4], who introduced parallel residual networks alongside the ViT backbone. A significant advancement came from Jia et al. [33], who proposed Visual Prompt Tuning (VPT). This method introduces learnable tokens called *visual prompts* at the input level of each ViT layer, effectively aligning downstream task distributions with pre-training data distributions through learnable data-level representations. Building on this foun-

dation, Yoo et al. [85] and Han et al. [24] further enhanced VPT by implementing cross-layer prompt connections with dynamic gating mechanisms, enabling adaptive control of prompt positioning and quantity.

However, existing VPT approaches primarily focus on manipulating prompt connections and structure, while overlooking the intrinsic relationship between prompts and data representations. Specifically, current VPT and its related methods [24, 33, 60, 85] initialize prompts randomly and optimize them solely through downstream task objectives. Although recent work [82] demonstrates improved learning efficiency through data-driven prompt initialization, the potential of leveraging discriminative and class-aware information remains largely unexplored. To deepen our understanding of prompt functionality and distribution, we investigate prompt-token relationships by addressing a fundamental question: **Could prompts be guided to facilitate information flow between image and class tokens to enhance representation learning?**

To address this question, we introduce a novel method that guides VPT optimization by leveraging semantic connections between visual prompts, visual tokens, and class tokens. We propose connecting prompts and visual data by constructing and learning a semantic metric between them in the deep layers of the ViT. For each prompt in these layers, we establish a semantic connection with its closest labeled class. As illustrated in Figure 1, we construct a semantic metric in the latent space by comparing prompts with corresponding image patches. Specifically, we aim to minimize the distance between visual prompts and visual tokens of the same class while maximizing separation from the visual tokens of different classes. We also apply a similar semantic metric between class tokens and prompts.

Our key insight is to increase the likelihood that prompts capture semantic information from same-class visual tokens while filtering out unrelated information. Through semantic metrics in both visual feature and prompt spaces, we demonstrate the effective transfer of relevant semantic information from visual tokens to class tokens via class-specific prompts. In other words, our framework employs related prompts as a *bridge* to connect class tokens and image patch semantic information through guided attention maps.

Extensive experiments across 24 visual recognition tasks in both Fine-Grained Visual Classification (FGVC) [33] and Visual Task Adaptation Benchmark (VTAB-1k) [87] demonstrate substantial improvements over standard VPT. Our method shows consistent effectiveness with both supervised and self-supervised pre-trained models, including MoCo and MAE. Additional evaluations on segmentation tasks further confirm that our approach significantly improves prompt learning efficiency and downstream task performance while requiring fewer prompts and learnable parameters compared to baseline VPT and its related state-of-the-art methods. Our

main contributions are:

- We propose **Distribution Aware Visual Prompt Tuning (DA-VPT)**, a novel framework that enhances prompt learning by constructing semantic metrics between prompts and corresponding image feature patches in deep ViT layers.
- We demonstrate that prompts can effectively bridge semantic information between image patches and class tokens through the attention mechanism, highlighting the importance of guided prompt learning.
- We validate our method’s effectiveness through extensive experiments on 24 visual recognition tasks and 2 segmentation tasks, showing significant improvements over vanilla VPT and its related works for both supervised and self-supervised pre-trained vision models.

2. Related Works

Parameter-Efficient Fine-Tuning (PEFT)

Transformers, initially introduced by Vaswani et al. [75], have revolutionized various domains through pre-training, from natural language processing (e.g., LLaMA [71], GPT [2]) to computer vision (e.g., MAE [28], CLIP [62], ViT-22b [12]). PEFT approaches have emerged to address the computational challenges of fine-tuning these large models by selectively updating only a subset of parameters. Early work by Kornblith et al. [38] focused on training only the classification head, while Zaken et al. [86] demonstrated significant improvements by tuning bias terms alone. Lian et al. [45] and Xie et al. [84] further refined these approaches by introducing adjustable shifting and scaling factors. Another significant direction in PEFT, pioneered by Houlsby et al. [31], involves incorporating lightweight adapter modules alongside Transformer backbones.

Visual Prompt Tuning (VPT) As a prominent branch of PEFT, prompt tuning introduces learnable tokens alongside input data to incorporate task-specific information [43, 44, 46, 47]. Jia et al. [33] pioneered the application of prompts in Vision Transformers (ViT), introducing VPT-Shallow for input layer modification and VPT-Deep for cross-layer integration. This foundational work catalyzed numerous developments in the field: Gao et al. [20] adapted visual prompts for test-time domain adaptation, while Gao et al. [18] extended the approach to video recognition. Subsequent studies enhanced VPT’s capabilities through dynamic mechanisms for optimizing prompt quantity and placement [24, 85], direct connections between intermediate layers and task-specific heads [73], and spatial selection mechanisms for coordinating attention between image patches and visual prompts [60].

Integration of PEFT Approaches While recent comprehensive approaches have demonstrated success in combining multiple PEFT methods [3, 89], our work focuses specifically on integrating bias optimization with VPT, which we empirically found to be sufficiently effective for demonstrat-

ing our method’s capabilities. A comprehensive evaluation of combinations with other PEFT methods lies beyond the scope of this work.

Metric Learning (ML) Metric Learning focuses on learning representations that effectively capture similarities and differences between data samples in the embedding space. Early approaches employed *contrastive loss* to differentiate between class samples [8, 23]. This evolved into *triplet loss* methods that introduce an *anchor* point as a proxy to simultaneously compare positive and negative samples with specified margins [6, 36, 65].

Advanced metric learning techniques have incorporated *Neighbourhood Components Analysis (NCA)* to better understand data distributions and class relationships [36, 53, 67, 68, 70, 78]. Recent studies have demonstrated particular success in applying NCA-based metric learning to Vision Transformer architectures [16, 39, 59], emphasizing the crucial role of data distributions in learning discriminative representations [41, 64, 65, 80]. Further investigations by Tsai et al. [72] and Ren et al. [66] have explored the integration of visual prompts with robust visual perception and deep metric learning.

Building on metric learning, our work examines the interactions between visual prompts, visual tokens, and class tokens within ViTs. We bridge the gap between traditional metric learning techniques and modern visual prompt tuning methods, offering a more principled way to optimize prompt-based transfer learning.

3. Methodology

3.1. Preliminary

The Vision Transformer (ViT) [14] is a fundamental model architecture that applies the original Transformer model [76] to computer vision tasks. Given an input image $\mathbf{I} \in \mathbb{R}^{H \times W \times C}$, ViT divides it into a sequence of N flattened 2D patches, which are then linearly projected into a D -dimensional embedding space. A learnable [CLS] (Class) token $\mathbf{x}_{\text{cls}} \in \mathbb{R}^D$ is prepended to the patch embeddings, serving as a global representation for classification tasks. The resulting sequence of embeddings $\mathbf{X} \in \mathbb{R}^{(N+1) \times D}$ is then passed through L Transformer block layers, where $l \in \{1, \dots, L\}$ denotes the layer index. Each layer consists of a Multi-Head Self-Attention (MHSA) mechanism defined as $\text{MHSA}(\mathbf{X}^l) = \text{Concat}(\mathbf{H}_1, \dots, \mathbf{H}_h)$, where each head \mathbf{H}_i computes a scaled dot-product attention $\text{softmax}(\frac{\mathbf{Q}\mathbf{K}^T}{\sqrt{d}}\mathbf{V})$ with subspaces of Query (\mathbf{Q}), Key (\mathbf{K}), and Value (\mathbf{V}) matrices projected from input embedding \mathbf{X}^{l-1} in the previous layer. The final output is the [CLS] token $\mathbf{x}_{\text{cls}}^L$, used for downstream classification tasks.

Visual Prompt Tuning (VPT) [33] presents a promising PEFT technique for ViT that adapts the pre-trained model to downstream tasks by introducing a small set of

learnable parameters, namely *visual prompts*. In a specific ViT block layer, a sequence of M learnable prompt tokens $\mathbf{P} = \{\mathbf{p}_1, \dots, \mathbf{p}_M\} \in \mathbb{R}^{M \times D}$ is concatenated with the patch embeddings $\mathbf{X} = \{\mathbf{x}_1, \dots, \mathbf{x}_N\} \in \mathbb{R}^{N \times D}$. Jia et al. [33] propose two VPT settings: **VPT-Shallow** where the prompts are only inserted into the first ViT layer, and **VPT-Deep** where the prompts are appended into every ViT layer. We follow the **VPT-Deep** setting since it has a higher capacity and aligns with our proposed method. The resulting sequence of embeddings $[\mathbf{x}_{\text{cls}}, \mathbf{P}, \mathbf{X}] \in \mathbb{R}^{(M+N+1) \times D}$ is then processed by the next ViT encoder layers. For layer l , the output of the $(l+1)$ -th layer can be described as:

$$[\mathbf{x}_{\text{cls}}^{l+1}, [\], \mathbf{x}_1^{l+1} \dots \mathbf{x}_N^{l+1}] = \text{BLK}([\mathbf{x}_{\text{cls}}^l, \mathbf{p}_1^l \dots \mathbf{p}_M^l, \mathbf{x}_1^l \dots \mathbf{x}_N^l]), \quad (1)$$

where $\mathbf{p}_1^l \dots \mathbf{p}_M^l$ are the M prompts in layer l , BLK represents the transformer block, and $[\]$ represents the position reserved for prompts in the next layer. During fine-tuning, only the visual prompts \mathbf{P} and the linear classification head are updated.

Metric Learning (ML) aims to learn a distance metric that captures semantic similarity between data points. The *Neighborhood Component Analysis (NCA)* [68] encourages learned embeddings to have a higher probability of correct classification by nearest neighbor classifiers. Given a set of N labeled data points $\{(\mathbf{x}_i, y_i)\}_{i=1}^N$, where $\mathbf{x}_i \in \mathbb{R}^D$ is the input feature vector and $y_i \in \{1, \dots, C\}$ is the corresponding class label from C classes, the NCA objective is:

$$\mathcal{L}_{\text{NCA}} = - \sum_{i=1}^N \log \frac{\sum_{j \in \mathcal{N}_i} \exp(-D(\mathbf{x}_i, \mathbf{x}_j)/\tau)}{\sum_{k \neq i} \exp(-D(\mathbf{x}_i, \mathbf{x}_k)/\tau)}, \quad (2)$$

where $\mathcal{N}_i = \{j \mid y_j = y_i, j \neq i\}$ denotes the set of neighboring points with the same class, $\tau > 0$ is the temperature parameter, and $D(\cdot, \cdot)$ represents the *cosine similarity*: $D(\mathbf{x}_i, \mathbf{x}_j) = \hat{\mathbf{x}}_i \cdot \hat{\mathbf{x}}_j$ where $\hat{\mathbf{x}} = \frac{\mathbf{x}}{\|\mathbf{x}\|_2}$ represents the L2-normalized vector. Following NCA, recent works [36, 70] introduce learnable class representations $\mathbf{P} = \{\mathbf{p}_i \in \mathbb{R}^D\}_{i=1}^C$, named *proxies*, to represent the C classes. In our work, we propose using prompts in deep layers as proxies for subsets of semantically similar classes.

3.2. Metric Learning on the Learnable Prompts

Our objective is to establish a metric in the feature space that quantifies the distance between learnable prompts and either visual tokens or the [CLS] token. We hypothesize that within each layer, a specific prompt should selectively capture information from a subset of relevant classes rather than searching indiscriminately across the entire class space. This targeted approach enables prompts to become more discriminative in their feature extraction while optimizing the [CLS] token’s ability to aggregate task-specific information from each class effectively. While this structured

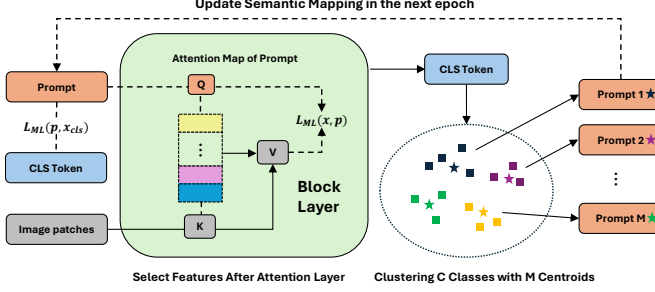


Figure 2. **Framework Overview.** Our method establishes semantic prompt-class mappings by clustering class representations into M clusters (M = number of prompts). Prompts are guided through a metric space using smoothed proxy NCA loss \mathcal{L}_{ML} between prompts and attention-based output tokens, enabling each prompt to capture information from its assigned semantic cluster. A similar metric guides [CLS] token-prompt relationships. The semantic mapping updates after each epoch, optimizing prompt distribution to capture fine-grained class-specific features.

information capture may differ from the emergent behavior of standard visual prompts, our empirical results demonstrate that metric learning guidance enhances model transferability, particularly when applied to deeper layers.

For a ViT block BLK_l at layer l ($l > 0$), we regularize the learning of prompts \mathbf{P}^l by constructing a space metric between the normalized prompts $\hat{\mathbf{p}}_k^l$ and normalized visual tokens $\hat{\mathbf{x}}_i^l$. For each prompt $\hat{\mathbf{p}}_k^l \in \mathbf{P}^l$ with assigned class label y_k , we aim to satisfy the following constraint for visual token samples $\hat{\mathbf{x}}_i^l$ and $\hat{\mathbf{x}}_j^l$ in the same batch with class different labels y_i and y_j respectively, where $\hat{\mathbf{x}}_i^l$ shares the same class label $y_i = y_k$ with $\hat{\mathbf{p}}_k^l$:

$$\hat{\mathbf{p}}_k^l \cdot \hat{\mathbf{x}}_i^l - \delta \geq \hat{\mathbf{p}}_k^l \cdot \hat{\mathbf{x}}_j^l + \delta \quad \forall i, j, k, y_k = y_i \neq y_j, \quad (3)$$

where \cdot denotes the dot product and $\delta > 0$ is the pre-defined margin. This constraint ensures that the cosine similarity between a prompt and tokens of the same class is greater than the similarity with tokens of different classes. Since cosine similarity naturally aligns with attention map comparison between Query and Key vectors, we argue that pairs $(\mathbf{p}_k, \mathbf{x}_i)$ that are closer in the spherical space will have higher probability of matching in the optimized attention map.

To efficiently build a metric space satisfying this constraint, we adopt the ML loss from Kim et al. [36], comparing learnable prompts with visual tokens using smoothed NCA loss (Proxy-Anchor loss). Our metric guidance objective between visual tokens \mathbf{X}^l and prompts \mathbf{P}^l is:

$$\mathcal{L}_{ML}(\mathbf{X}, \mathbf{P}) = \frac{1}{|\mathcal{P}^+|} \sum_{\mathbf{p}_k \in \mathcal{P}^+} \left[\text{LSE}_0^+ \left(-(\hat{\mathbf{p}}_k \cdot \hat{\mathbf{x}}_i - \delta) / \tau \right) \right] + \frac{1}{|\mathcal{P}|} \sum_{\mathbf{p}_k \in \mathcal{P}} \left[\text{LSE}_0^+ \left((\hat{\mathbf{p}}_k \cdot \hat{\mathbf{x}}_j + \delta) / \tau \right) \right], \quad (4)$$

where $\text{LSE}_0^+(x) = \log(1 + \sum_{i=1}^N e^{x_i})$ is the smoothed LogSumExp with first argument set to 1, \mathcal{P} denotes the set of all prompts, \mathcal{P}^+ denotes the set of positive prompts where same-class data exists in the minibatch, \mathcal{X}_p^+ denotes the set of visual tokens with the same label as the selected prompt \mathbf{p} , and \mathcal{X}_p^- is its complement set. In practice, we found that comparing the projected Query vector $\mathbf{Q} = \mathbf{P}^l \mathbf{W}_Q^l$ yields better performance, where $\mathbf{W}_Q^l \in \mathbb{R}^{D \times D}$ is the Query projection matrix at layer l .

We also propose a similar loss $\mathcal{L}_{ML}(\mathbf{P}, \mathbf{x}_{cls})$ that pulls the [CLS] token closer to corresponding prompts while pushing it away from prompts of different classes. The overall loss becomes:

$$\mathcal{L} = \mathcal{L}_{CE} + \beta \mathcal{L}_{ML}(\mathbf{X}, \mathbf{P}) + \lambda \mathcal{L}_{ML}(\mathbf{P}, \mathbf{x}_{cls}), \quad (5)$$

where $\beta, \lambda > 0$ are hyperparameters. By jointly optimizing both metric learning terms, our method encourages prompts to capture class-specific information and aligns the [CLS] token with relevant prompts.

3.3. Projection and Saliency Patch Selection

To ensure prompts effectively focus on critical image information while filtering out false positive visual tokens, we propose selecting saliency information from visual tokens as positive and negative samples for prompt comparison in $\mathcal{L}_{ML}(\mathbf{X}, \mathbf{P})$. While extracting saliency patches directly from attention maps is straightforward, it can be computationally intensive, especially with optimized attention mechanisms like Flash Attention. Instead, as shown in Figure 2, we use the output representation immediately following the attention layer. The output representation $\mathbf{X}^l = \text{MHSA}(\mathbf{X}^l) \in \mathbb{R}^{N \times D}$ then concatenates representations from each head, serving as a saliency aggregation of visual tokens.

3.4. Dynamically Mapping Classes and Prompts

We set M learnable prompts in each layer where $M \ll C$ to avoid optimization difficulties and unequal training opportunities. We develop a semantic mapping strategy to map C classes to M prompts. Before training, we run an additional epoch to obtain class representations $\mathbf{S} \in \mathbb{R}^{C \times D}$ by mean-pooling the [CLS] token for each class using the pre-trained ViT. We then use k-means clustering to group these representations into M clusters, assigning classes to prompts based on cluster membership, as shown in Figure 2.

To maintain semantic mapping accuracy, we update the mapping after each epoch. During training, we collect and calculate updated class representations \mathbf{S} , then update k-means using previous epoch centroids as initialization to adjust the class-prompt mapping.

3.5. Efficient Bias Tuning

To further improve the flexibility in the distribution of visual tokens, we investigate the partial release of ViT backbone bias terms as suggested by Zaken et al. [86]. We found that fine-tuning performance significantly improves when bias terms are partially enabled with our metric guidance loss. The most efficient components are the bias terms $\mathbf{b}_K, \mathbf{b}_V \in \mathbb{R}^D$ in the Key and Value linear projections of the self-attention mechanism (Figure 4b). This observation aligns with findings from Zaken et al. [86] and Cordonnier et al. [10]. Partially allowing bias terms to adapt provides additional flexibility in adjusting visual token distributions and capturing task-specific information under metric guidance.

4. Technical Discussion

4.1. Connection Between Similarity and Attention

In this section, we analyze how changes in token similarity influence attention weights through gradient updates. Specifically, we examine how a small change in the similarity between a prompt \mathbf{p} and a visual token \mathbf{x}_i affects the corresponding attention weight a_i . Let $\Delta\mathbf{p}$ represent a small perturbation that brings \mathbf{p} closer to \mathbf{x}_i in the embedding space. We formalize this relationship in the following theorem:

Theorem 1 (Attention-Similarity Relationship). *For an attention weight perturbation Δa_i computed using the softmax function, the following approximation holds:*

$$\Delta a_i \approx a_i(1 - a_i)\Delta s_i, \quad (6)$$

where Δs_i represents the change in attention score s_i , given by $\Delta s_i = \frac{\Delta\mathbf{p}^\top \mathbf{x}_i}{\sqrt{d}}$, and d is the dimension of the attention head.

This approximation reveals that a positive gradient change in attention weight ($\Delta a_i > 0$) occurs when:

$$a_i(1 - a_i)\Delta s_i = a_i(1 - a_i)\frac{\Delta\mathbf{p}^\top \mathbf{x}_i}{\sqrt{d}} > 0 \quad (7)$$

This condition is satisfied when \mathbf{p} moves closer to \mathbf{x}_i in the embedding space. Conversely, when \mathbf{p} moves away from \mathbf{x}_i , Δa_i decreases. This theorem establishes a direct connection between token similarity and attention mapping, demonstrating how our metric learning guidance influences attention through token distribution. The complete proof is provided in the Appendix.

4.2. Analysis of Guided Attention Maps

To further analyze the impact of our metric guidance loss on fine-tuning, we visualize attention maps between visual tokens and prompts across different layers (Figure 3a). Our analysis reveals distinct patterns:

(1) In Shallow Layers:

- Both VPT-Deep and our method show prompts attending to different object subregions
- Our method demonstrates enhanced diversity and precision in information capture

(2) In Deep Layers:

- Attention maps become sparser as token representations become more abstract
- Standard VPT-Deep prompts show limited information selection compared to the [CLS] token
- Our positive prompt ($\ast\mathbf{p}$) successfully identifies informative patches that are subsequently selected by the [CLS] token

These visualizations demonstrate that positively labeled prompts serve as effective "bridges" for semantic information flow to the [CLS] token in deep layers. As shown in Figure 3b, our DA-VPT enables prompts to aggregate discriminative features from same-class data, resulting in more fine-grained attention patterns compared to the baseline. This enhanced information routing significantly improves the model's discriminative capability during fine-tuning.

Artifact Consideration: Recent work by Darcet et al. [11] revealed the existence of attention artifacts in vision transformers, which we also observe in our prompt attention maps (Figure 3a). While they demonstrate that training with *registers* (analogous to learnable prompts) from scratch can eliminate these artifacts, both standard VPT and our method exhibit them due to prompt introduction during fine-tuning rather than pre-training. Nevertheless, our comparative analysis shows that the proposed guidance mechanism reduces both the frequency and spread of artifacts, constraining them more effectively within semantic object boundaries. While our method achieves better alignment between attention patterns and object semantics, the nature and impact of these artifacts on model performance presents an intriguing avenue for future investigation.

4.3. Compatibility with Metric Learning Methods

Our selection of the *Proxy-Anchor* method [36] is motivated by its natural alignment with our hypothesized role of visual prompts, where both proxies and prompts serve as class representatives and comparative anchors for data tokens. Alternative metric learning approaches, such as *Proxy-NCA* [70] and conventional *triplet loss* [6, 30], treat all representations as equal data points. These approaches are less suitable for our framework because the significant disparity between the number of visual prompts (M) and data tokens (N , where $M \ll N$) creates an *unbalanced opti-*

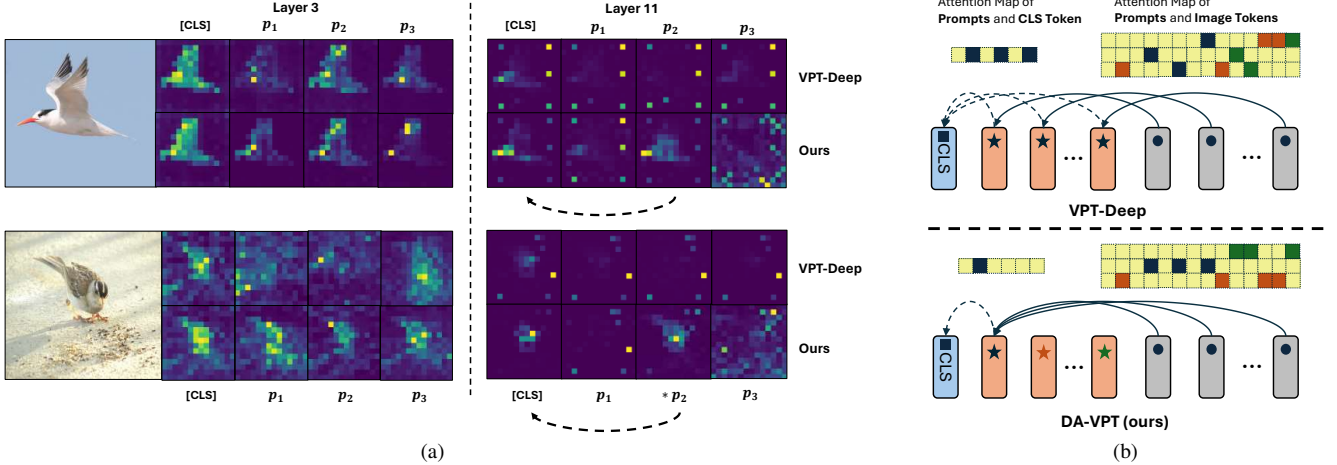


Figure 3. Comparison of attention patterns between VPT-Deep and our method on CUB dataset samples. (a) Attention maps in shallow (layer 3) and deep (layer 11) layers, showing CLS token and sampled prompt attention patterns. In layer 11, $*p$ indicates the prompt guided as positive to the CLS token, while others represent negative prompts. Additional visualization examples are provided in Appendix. (b) Information flow comparison between baseline VPT-Deep and our DA-VPT. Our method enables selected prompts to aggregate and transfer fine-grained details from same-class visual tokens to the [CLS] token more effectively.

mization problem. Our empirical studies further confirm this theoretical intuition: attempting to fine-tune with conventional metric learning methods leads to training instability, whereas the Proxy-Anchor formulation maintains stable optimization by explicitly accounting for the asymmetric nature of prompt-token relationships.

5. Experiments

5.1. Experimental Setup

Datasets. We evaluate our method on three types of visual transfer learning tasks. For visual recognition, we use the Fine-Grained Visual Classification (FGVC) benchmark [33] comprising 5 datasets. For few-shot transfer learning, we employ the Visual Task Adaptation Benchmark (VTAB-1K) [87] containing 19 datasets. Additionally, we evaluate dense prediction tasks on ADE20K [91] and PASCAL Context [52]. Detailed dataset characteristics and experimental settings are provided in the Appendix.

Model Architecture. We employ Vision Transformer (ViT) [14] as our backbone, using the base model **ViT-B** (12 layers) for visual classification tasks and the large model **ViT-L** (24 layers) for semantic segmentation. To evaluate generalization, we initialize the backbone using either supervised pre-training on ImageNet-21K [13] or self-supervised pre-training on ImageNet-1K using methods such as MoCo v3 [5] and MAE [27].

Method Variants. We evaluate two versions of our approach. Our primary method, **DA-VPT**, builds on VPT-Deep [33] while incorporating our proposed metric learning losses $\mathcal{L}_{ML}(\mathbf{X}, \mathbf{P})$ and $\mathcal{L}_{ML}(\mathbf{P}, \mathbf{x}_{cls})$. The enhanced version, **DA-VPT+**, further incorporates efficient bias tuning as detailed in Section 3.5.

Implementation Details. For all experiments, we conduct extensive hyperparameter optimization, including learning rate, parameter decays, and the number of visual prompts for layers both with and without our metric learning guidance. Through this empirical investigation, we identified that the optimal number of prompts for most downstream tasks is approximately 20. For metric learning parameters, we adopt the Proxy-Anchor defaults with margin $\delta = 32$ and temperature $\tau = 10$. Extended experimental details, including hyperparameter studies and ablation analyses, are provided in the Appendix.

5.2. Result Comparison with the State-of-the-Art

We evaluate our method against existing VPT-based and recent related approaches across 24 vision tasks. As shown in Table 1, our DA-VPT+ consistently achieves superior performance over VPT-related methods on both supervised ViT and self-supervised backbones. On ViT-B, DA-VPT+ improves over the VPT-Deep baseline by 2.83 and 4.18 percentage points (pp) on FGVC and VTAB-1K, respectively, and outperforms E2VPT by 2.72 pp and 2.20 pp on these tasks. Notably, even without bias tuning, DA-VPT maintains strong results across major benchmarks. The improvements are particularly pronounced with self-supervised backbones, where our method also surpasses full fine-tuning on all backbones while using fewer parameters. These results highlight the effectiveness and generalizability of our approach across diverse downstream tasks compared to other VPT-based methods.

Table 2 demonstrates our proposed methods, DA-VPT and DA-VPT+, achieve significant improvements over existing baselines and recent competitive methods in semantic segmentation tasks on both the ADE20K and PASCAL Con-

Methods	Mean	FGVC	VTAB-1K			
	Param (M)	Mean Acc (5)	Natural (7)	Specialized (4)	Structured (8)	Mean Acc
ViT-B with Supervised pretrained on ImageNet-21k						
Full	85.98	88.54	75.88	83.36	47.64	68.96
VPT-Shallow	0.11	84.62	76.81	79.68	46.98	67.82
VPT-Deep	0.64	89.11	78.48	82.43	54.98	71.96
E2VPT [24]	0.33	89.22	80.01	84.43	57.39	73.94
DA-VPT (ours)	0.21	91.22	80.25	85.12	58.71	74.69
DA-VPT+ (ours)	0.24	91.94	81.98	86.47	59.96	76.14
ViT-B with MAE pretrained on ImageNet-1K						
Full	85.8	82.80	59.31	79.68	53.82	64.27
VPT-Shallow	0.10	57.84	39.96	69.65	27.50	45.70
VPT-Deep	0.20	72.02	36.02	60.61	26.57	41.73
GateVPT [85]	0.17	73.39	47.61	76.86	36.80	53.09
E2VPT [24]	0.06	—	59.52	77.80	44.65	60.66
DA-VPT (ours)	0.20	82.17	62.14	79.14	54.31	65.19
DA-VPT+ (ours)	0.22	83.20	66.59	82.96	59.28	69.61
ViT-B with MoCo-V3 pretrained on ImageNet-1K						
Full	85.8	84.25	71.95	84.72	51.98	69.55
VPT-Shallow	0.11	79.26	67.34	82.26	37.55	62.38
VPT-Deep	0.20	83.12	70.27	83.04	42.38	65.90
GateVPT [85]	0.17	83.00	74.84	83.38	49.10	69.11
E2VPT [24]	0.11	—	76.47	87.28	54.91	72.88
DA-VPT (ours)	0.21	85.02	74.24	83.21	55.23	70.90
DA-VPT+ (ours)	0.24	86.16	76.86	84.71	58.98	73.53

Table 1. **Comparison of Fine-tuning Methods.** Performance evaluation across 24 vision tasks (5 FGVC and 19 VTAB-1K) using supervised ViT and self-supervised backbones (MAE [27], MoCo-v3 [5]). Detailed per-task results for VTAB-1K are provided in Appendix.

Method	#Param	ADE20K		PASCAL Context	
		mIoU-SS	mIoU-MS	mIoU-SS	mIoU-MS
Full-Tuning	317.3M	47.60	49.18	53.69	55.21
Linear	13.1M	38.09	39.16	46.06	48.13
Bias	13.2M	43.61	45.73	45.15	46.47
VPT (baseline)	13.6M	44.08	46.01	49.51	50.46
SPT-LoRA [25]	14.6M	45.40	47.50	—	—
SPT-Adapter [25]	14.6M	45.20	47.20	—	—
DA-VPT (ours)	13.6M	45.10	47.07	50.15	51.04
DA-VPT+ (ours)	13.7M	46.47	47.21	50.40	51.28

Table 2. **Results of Semantic Segmentation on ADE20K and PASCAL Context.** We report mIoU-SS (single-scale inference) and mIoU-MS (multi-scale inference). All experiments use the ViT-L backbone pre-trained on ImageNet-21K. The #Param column indicates the total number of tunable parameters in the entire framework. For SPT [25], we report the results from the original paper, while for other settings and our baseline, we provide our reproduced results. We highlight the best results other than the full fine-tuning.

text datasets. Compared to classification tasks, dense prediction tasks such as segmentation are much more challenging. Notably, lightweight PEFT methods like Linear or Bias exhibit low efficiency compared to full fine-tuning. In such challenging tasks, our proposed DA-VPT+ still achieves comparable performance while using only 4.3% of the tunable parameters, demonstrating both high parameter efficiency and effectiveness across both datasets.

Table 3 compares state-of-the-art PEFT methods on FGVC [33] using ImageNet-21K pre-trained ViT-B. Our DA-VPT+ achieves the highest mean accuracy of 91.94% across all datasets, surpassing previous SOTA methods SNF [81] and MoSA [88] on FGVC. Notable improvements include gains of 0.6 and 1.8 percentage points on CUB and Cars datasets respectively. Both DA-VPT and DA-VPT+

Method	Dataset	CUB-200 -2011	NABirds	Oxford Flowers	Stanford Dogs	Stanford Cars	Mean Acc (%)	Mean Params (M)
Full fine-tuning [33]		87.3	82.7	98.8	89.4	84.5	88.54	85.98
Linear Probing [33]		85.3	75.9	97.9	86.2	51.3	79.32	0.18
Adapter [31]		87.1	84.3	98.5	89.8	68.6	85.67	0.41
Bias [86]		88.4	84.2	98.8	91.2	79.4	88.41	0.28
AdaptFormer [4]		87.4	84.8	99.0	90.7	81.0	88.58	1.54
VPT-Shallow [33]		86.7	78.8	98.4	90.7	68.7	84.62	0.25
VPT-Deep [33]		88.5	84.2	99.0	90.2	83.6	89.11	0.85
SSF [45]		89.5	85.7	99.6	89.6	89.2	90.72	0.39
SNF [81]		90.2	87.4	99.7	89.5	86.9	90.74	0.25
MP [19]		89.3	84.9	99.6	89.5	83.6	89.38	1.20
E2VPT [24]		89.1	84.6	99.1	90.5	82.8	89.22	0.65
MoSA [88]		89.3	85.7	99.2	91.9	83.4	89.90	1.54
VPT (Baseline)		88.6	85.7	99.2	89.0	87.4	90.14	0.36
DA-VPT (Ours)		90.2	87.4	99.4	89.4	89.7	91.22	0.30
DA-VPT+ (Ours)		90.8	88.3	99.8	89.8	91.0	91.94	0.32

Table 3. **Comparison of various fine-tuning methods on different downstream tasks.** The ViT-B model pre-trained on ImageNet-21K is used as basic backbone. Top-1 accuracy (%) is reported and the best result is in bold.

outperform the VPT baseline and full fine-tuning with significant margin while using fewer parameters, demonstrating superior accuracy-efficiency trade-off compared to full fine-tuning and existing PEFT methods.

5.3. Ablation Studies and Discussion

5.3.1. Ablation Study

The ablation study demonstrates the individual and collective contributions of each component in our proposed DA-VPT method on the CUB dataset from the FGVC benchmark and the Natural task category from the VTAB-1k benchmark. The metric learning losses, $\mathcal{L}_{ML}(\mathbf{x}, \mathbf{p})$ and $\mathcal{L}_{ML}(\mathbf{p}, \mathbf{x}_{cls})$, lead to accuracy improvements of 1.08 *pp* on VTAB-1k Natural and 1.22 *pp* on CUB over the baseline. The integration of Efficient Bias further enhances the performance, contributing to an additional 0.97 *pp* and 1.03 *pp* improvement on the respective datasets. When all three components are combined, our DA-VPT method achieves the highest performance, with total accuracy improvements of 2.05 *pp* on VTAB-1k Natural and 2.25 *pp* on CUB.

While the incorporation of these components introduces a minimal increase in latency and memory usage, the gained accuracy far outweighs this slight trade-off. Note that the combination of $\mathcal{L}_{ML}(\mathbf{x}, \mathbf{p})$, $\mathcal{L}_{ML}(\mathbf{p}, \mathbf{x}_{cls})$ and Efficient Bias yields substantial improvements with only a modest increase in parameters. This highlights the efficiency of our method in achieving significant performance gains with minimal parameter overhead.

5.3.2. Analysis of Parameter Impacts

Layer-wise Impact. We first examine the effectiveness of our metric learning loss when applied to different layers. As shown by the blue line in Figure 4a, applying the loss to the final layer yields optimal results in most cases, likely due to the presence of higher-level semantic features in deeper layers. We further investigate the effect of applying our loss across multiple consecutive layers, represented by the

Table 4. **Ablation study on different components in our DA-VPT on two datasets: CUB-200-2011 in FGVC and *Natural* in VTAB-1k.** For each \mathcal{L}_{ML} component, we also search for its optimal hyperparameter. The learnable [CLS] token is combined with Efficient Bias for simplicity. We fixed the number of prompts to 20 for all settings. The latency and memory are tested in the same server with RTX4090 GPU.

Components of our Techniques			VTAB-1k <i>Natural</i> (7)		FGVC CUB-200		Latency (ms/img)	Memory (GB)
$\mathcal{L}_{ML}(\mathbf{x}, \mathbf{p})$	$\mathcal{L}_{ML}(\mathbf{p}, \mathbf{x}_{cls})$	Efficient Bias	Param	Accuracy	Param	Accuracy		
				79.45 (base)		88.64 (base)	1.41	2.41
✓			0.14M (0.16%)	79.47 (+0.02) 79.51 (+0.06) 80.53 (+1.08)	0.20M (0.24%)	89.24 (+0.60) 89.06 (+0.42) 89.86 (+1.22)	1.51 1.52 1.54	2.41 2.41 2.41
✓	✓	✓	0.16M (0.19%)	80.06 (+0.61) 81.02 (+1.57) 81.50 (+2.05) 81.98 (+2.53)	0.23M (0.27%)	89.55 (+0.91) 90.41 (+1.77) 90.54 (+1.90) 90.89 (+2.25)	1.45 1.53 1.53 1.56	2.76 2.76 2.76 2.76

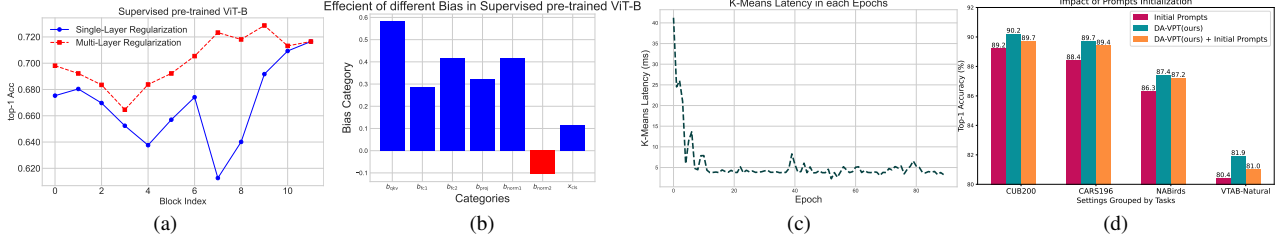


Figure 4. **4a** Illustrates the impact of the number and position of the layers to which the proposed metric learning loss is applied. **4c** This figure shows the latency of the k-means calculation in each epoch. **4b** Illustrates the importance of each category of efficient bias measured on the CUB-200-2011 dataset. **4d** This figure shows the comparison of the performance with or without the prompts initialization with data mean value.

red line, which shows the performance when applying the loss from a specific layer through to the final layer. The impact varies notably across different pre-trained models, with detailed results for MAE and MoCo provided in the Appendix.

Efficient Bias Components. Figure 4b demonstrates that specific categories of efficient bias contribute disproportionately to performance improvements. This observation underscores the importance of selective optimization of bias components rather than uniform adjustment across all parameters.

Semantic Mapping Updates. The computational cost of k-means clustering for semantic mapping updates is illustrated in Figure 4c. Notably, while the initial epochs incur higher computational overhead, the latency decreases significantly in later epochs as class representations stabilize. This suggests that the computational cost of maintaining dynamic class-prompt mappings becomes negligible as training progresses.

Prompt Initialization. We investigate the impact of prompt initialization by comparing mean value initialization on both baseline VPT and our proposed DA-VPT, following the methodology of Wang et al. [82], where prompts are initialized with *mean pooling* values from the dataset at each layer. As shown in Figure 4d, our analysis reveals that such initialization actually impedes our method’s effectiveness. We attribute this to the increased difficulty in

guiding prompts to capture discriminative information when initialized with homogeneous content from the mean value. Additional parameter impact analyses are provided in the Appendix.

6. Conclusion

This paper introduces Distribution-Aware Visual Prompt Tuning (DA-VPT), a novel framework that improves visual prompt learning in Vision Transformers (ViT) through semantic metric construction between prompts and image features. Our method guides prompts to serve as effective bridges for semantic information flow between image patches and class tokens via the attention mechanism. Extensive evaluations across 24 visual recognition and 2 segmentation tasks demonstrate that DA-VPT significantly outperforms vanilla VPT and other related methods while using fewer prompts and parameters. Our results highlight the importance of considering the intrinsic connection between visual prompts and data samples and showcase the potential of our approach to enhance the transfer learning capabilities of pre-trained vision models. We believe that our findings can inspire further research on parameter-efficient fine-tuning strategies and contribute to the development of more effective and efficient vision foundation models.

References

- [1] Charles Beattie, Joel Z Leibo, Denis Teplyashin, Tom Ward, Marcus Wainwright, Heinrich Küttler, Andrew Lefrancq, Simon Green, Víctor Valdés, Amir Sadik, et al. Deepmind lab. *arXiv preprint arXiv:1612.03801*, 2016. [13](#)
- [2] Tom Brown, Benjamin Mann, Nick Ryder, Melanie Subbiah, Jared D Kaplan, Prafulla Dhariwal, Arvind Neelakantan, Pranav Shyam, Girish Sastry, Amanda Askell, et al. Language models are few-shot learners. *NeurIPS*, 33:1877–1901, 2020. [2](#)
- [3] Arnav Chavan, Zhuang Liu, Deepak Gupta, Eric Xing, and Zhiqiang Shen. One-for-all: Generalized lora for parameter-efficient fine-tuning. *arXiv preprint arXiv:2306.07967*, 2023. [2](#)
- [4] Shoufa Chen, Chongjian Ge, Zhan Tong, Jiangliu Wang, Yibing Song, Jue Wang, and Ping Luo. Adaptformer: Adapting vision transformers for scalable visual recognition. *NeurIPS*, 2022. [1, 7](#)
- [5] Xinlei Chen, Saining Xie, and Kaiming He. An empirical study of training self-supervised vision transformers. In *CVPR*, pages 9640–9649, 2021. [6, 7](#)
- [6] De Cheng, Yihong Gong, Sanping Zhou, Jinjun Wang, and Nanning Zheng. Person re-identification by multi-channel parts-based cnn with improved triplet loss function. In *CVPR*, pages 1335–1344, 2016. [3, 5](#)
- [7] Gong Cheng, Junwei Han, and Xiaoqiang Lu. Remote sensing image scene classification: Benchmark and state of the art. *Proceedings of the IEEE*, pages 1865–1883, 2017. [13](#)
- [8] Sumit Chopra, Raia Hadsell, and Yann LeCun. Learning a similarity metric discriminatively, with application to face verification. In *CVPR*. IEEE, 2005. [3](#)
- [9] Mircea Cimpoi, Subhransu Maji, Iasonas Kokkinos, Sammy Mohamed, and Andrea Vedaldi. Describing textures in the wild. In *CVPR*, pages 3606–3613, 2014. [13](#)
- [10] Jean-Baptiste Cordonnier, Andreas Loukas, and Martin Jaggi. Multi-head attention: Collaborate instead of concatenate. *arXiv preprint arXiv:2006.16362*, 2020. [5](#)
- [11] Timothée Darcet, Maxime Oquab, Julien Mairal, and Piotr Bojanowski. Vision transformers need registers. *ICLR*, 2024. [5](#)
- [12] Mostafa Dehghani, Josip Djolonga, Basil Mustafa, Piotr Padlewski, Jonathan Heek, Justin Gilmer, Andreas Peter Steiner, Mathilde Caron, Robert Geirhos, Ibrahim Alabdulmohsin, et al. Scaling vision transformers to 22 billion parameters. In *ICML*, pages 7480–7512. PMLR, 2023. [2](#)
- [13] Jia Deng, Wei Dong, Richard Socher, Li-Jia Li, Kai Li, and Li Fei-Fei. Imagenet: A large-scale hierarchical image database. In *CVPR*, pages 248–255. Ieee, 2009. [1, 6](#)
- [14] Alexey Dosovitskiy, Lucas Beyer, Alexander Kolesnikov, Dirk Weissenborn, Xiaohua Zhai, Thomas Unterthiner, Mostafa Dehghani, Matthias Minderer, Georg Heigold, Sylvain Gelly, et al. An image is worth 16x16 words: Transformers for image recognition at scale. *arXiv preprint arXiv:2010.11929*, 2020. [1, 3, 6](#)
- [15] Emma Dugas, Jorge Jared, and Will Cukierski. Diabetic retinopathy detection, 2015. [13](#)
- [16] Aleksandr Ermolov, Leyla Mirvakhabova, Valentin Khrulkov, Nicu Sebe, and Ivan Oseledets. Hyperbolic vision transformers: Combining improvements in metric learning. In *CVPR*, pages 7409–7419, 2022. [3](#)
- [17] Li Fei-Fei, Robert Fergus, and Pietro Perona. One-shot learning of object categories. *IEEE TPAMI*, 28(4):594–611, 2006. [13](#)
- [18] Kaifeng Gao, Long Chen, Hanwang Zhang, Jun Xiao, and Qianru Sun. Compositional prompt tuning with motion cues for open-vocabulary video relation detection. *ICLR*, 2023. [2](#)
- [19] Mingze Gao, Qilong Wang, Zhenyi Lin, Pengfei Zhu, Qinghua Hu, and Jingbo Zhou. Tuning pre-trained model via moment probing. In *CVPR*, pages 11803–11813, 2023. [7, 12](#)
- [20] Yunhe Gao, Xingjian Shi, Yi Zhu, Hao Wang, Zhiqiang Tang, Xiong Zhou, Mu Li, and Dimitris N Metaxas. Visual prompt tuning for test-time domain adaptation. *arXiv preprint arXiv:2210.04831*, 2022. [2](#)
- [21] Timnit Gebru, Jonathan Krause, Yilun Wang, Duyun Chen, Jia Deng, and Li Fei-Fei. Fine-grained car detection for visual census estimation. In *AAAI*, 2017. [12, 13](#)
- [22] Andreas Geiger, Philip Lenz, Christoph Stiller, and Raquel Urtasun. Vision meets robotics: The kitti dataset. *The International Journal of Robotics Research*, pages 1231–1237, 2013. [13](#)
- [23] Raia Hadsell, Sumit Chopra, and Yann LeCun. Dimensionality reduction by learning an invariant mapping. In *CVPR*. IEEE, 2006. [3](#)
- [24] Cheng Han, Qifan Wang, Yiming Cui, Zhiwen Cao, Wenguan Wang, Siyuan Qi, and Dongfang Liu. E² 2vpt: An effective and efficient approach for visual prompt tuning. *arXiv preprint arXiv:2307.13770*, 2023. [2, 7](#)
- [25] Haoyu He, Jianfei Cai, Jing Zhang, Dacheng Tao, and Bohan Zhuang. Sensitivity-aware visual parameter-efficient fine-tuning. In *CVPR*, pages 11825–11835, 2023. [7](#)
- [26] Kaiming He, Haoqi Fan, Yuxin Wu, Saining Xie, and Ross Girshick. Momentum contrast for unsupervised visual representation learning. In *CVPR*, pages 9729–9738, 2020. [1](#)
- [27] Kaiming He, Xinlei Chen, Saining Xie, Yanghao Li, Piotr Dollár, and Ross Girshick. Masked autoencoders are scalable vision learners. In *CVPR*, pages 16000–16009, 2022. [1, 6, 7](#)
- [28] Kaiming He, Xinlei Chen, Saining Xie, Yanghao Li, Piotr Dollár, and Ross Girshick. Masked autoencoders are scalable vision learners. In *CVPR*, pages 16000–16009, 2022. [2](#)
- [29] Patrick Helber, Benjamin Bischke, Andreas Dengel, and Damian Borth. Eurosat: A novel dataset and deep learning benchmark for land use and land cover classification. *IEEE Journal of Selected Topics in Applied Earth Observations and Remote Sensing*, pages 2217–2226, 2019. [13](#)
- [30] Alexander Hermans, Lucas Beyer, and Bastian Leibe. In defense of the triplet loss for person re-identification. *arXiv preprint arXiv:1703.07737*, 2017. [5](#)
- [31] Neil Houlsby, Andrei Giurgiu, Stanislaw Jastrzebski, Bruna Morrone, Quentin De Laroussilhe, Andrea Gesmundo, Mona Attariyan, and Sylvain Gelly. Parameter-efficient transfer learning for nlp. In *ICML*, pages 2790–2799. PMLR, 2019. [1, 2, 7, 17](#)

- [32] Edward J Hu, Yelong Shen, Phillip Wallis, Zeyuan Allen-Zhu, Yuanzhi Li, Shean Wang, Lu Wang, and Weizhu Chen. Lora: Low-rank adaptation of large language models. *arXiv preprint arXiv:2106.09685*, 2021. 1
- [33] Menglin Jia, Luming Tang, Bor-Chun Chen, Claire Cardie, Serge Belongie, Bharath Hariharan, and Ser-Nam Lim. Visual prompt tuning. In *ECCV*, pages 709–727. Springer, 2022. 1, 2, 3, 6, 7, 12, 13, 17
- [34] Justin Johnson, Bharath Hariharan, Laurens Van Der Maaten, Li Fei-Fei, C Lawrence Zitnick, and Ross Girshick. Clevr: A diagnostic dataset for compositional language and elementary visual reasoning. In *CVPR*, pages 2901–2910, 2017. 13
- [35] Aditya Khosla, Nityananda Jayadevaprakash, Bangpeng Yao, and Fei-Fei Li. Novel dataset for fine-grained image categorization: Stanford dogs. In *Proc. CVPR workshop on fine-grained visual categorization (FGVC)*. Citeseer, 2011. 12, 13
- [36] Sungyeon Kim, Dongwon Kim, Minsu Cho, and Suha Kwak. Proxy anchor loss for deep metric learning. In *CVPR*, pages 3238–3247, 2020. 3, 4, 5
- [37] Alexander Kirillov, Eric Mintun, Nikhila Ravi, Hanzi Mao, Chloe Rolland, Laura Gustafson, Tete Xiao, Spencer Whitehead, Alexander C Berg, Wan-Yen Lo, et al. Segment anything. In *CVPR*, pages 4015–4026, 2023. 1
- [38] Simon Kornblith, Jonathon Shlens, and Quoc V Le. Do better imagenet models transfer better? In *CVPR*, pages 2661–2671, 2019. 1, 2
- [39] Dmytro Kotovenko, Pingchuan Ma, Timo Milbich, and Björn Ommer. Cross-image-attention for conditional embeddings in deep metric learning. In *CVPR*, pages 11070–11081, 2023. 3
- [40] Alex Krizhevsky, Geoffrey Hinton, et al. Learning multiple layers of features from tiny images. 2009. 13
- [41] Issam H Laradji and Reza Babanezhad. M-adda: Unsupervised domain adaptation with deep metric learning. *Domain adaptation for visual understanding*, pages 17–31, 2020. 3
- [42] Yann LeCun, Fu Jie Huang, and Leon Bottou. Learning methods for generic object recognition with invariance to pose and lighting. In *CVPR*. IEEE, 2004. 13
- [43] Brian Lester, Rami Al-Rfou, and Noah Constant. The power of scale for parameter-efficient prompt tuning. *arXiv preprint arXiv:2104.08691*, 2021. 2
- [44] Xiang Lisa Li and Percy Liang. Prefix-tuning: Optimizing continuous prompts for generation. *arXiv preprint arXiv:2101.00190*, 2021. 1, 2
- [45] Dongze Lian, Daquan Zhou, Jiashi Feng, and Xinchao Wang. Scaling & shifting your features: A new baseline for efficient model tuning. *Neurips*, 35:109–123, 2022. 2, 7, 12
- [46] Pengfei Liu, Weizhe Yuan, Jinlan Fu, Zhengbao Jiang, Hiroaki Hayashi, and Graham Neubig. Pre-train, prompt, and predict: A systematic survey of prompting methods in natural language processing. *ACM Computing Surveys*, 55(9):1–35, 2023. 2
- [47] Xiao Liu, Kaixuan Ji, Yicheng Fu, Weng Lam Tam, Zhengxiao Du, Zhilin Yang, and Jie Tang. P-tuning v2: Prompt tuning can be comparable to fine-tuning universally across scales and tasks. *arXiv preprint arXiv:2110.07602*, 2021. 2
- [48] Ilya Loshchilov and Frank Hutter. Sgdr: Stochastic gradient descent with warm restarts. *arXiv preprint arXiv:1608.03983*, 2016. 12
- [49] Ilya Loshchilov and Frank Hutter. Decoupled weight decay regularization. *arXiv preprint arXiv:1711.05101*, 2017. 12
- [50] Dhruv Mahajan, Ross Girshick, Vignesh Ramanathan, Kaiming He, Manohar Paluri, Yixuan Li, Ashwin Bharambe, and Laurens Van Der Maaten. Exploring the limits of weakly supervised pretraining. In *ECCV*, pages 181–196, 2018. 1
- [51] Loic Matthey, Irina Higgins, Demis Hassabis, and Alexander Lerchner. dsprites: Disentanglement testing sprites dataset, 2017. 13
- [52] Roozbeh Mottaghi, Xianjie Chen, Xiaobai Liu, Nam-Gyu Cho, Seong-Whan Lee, Sanja Fidler, Raquel Urtasun, and Alan Yuille. The role of context for object detection and semantic segmentation in the wild. In *CVPR*, pages 891–898, 2014. 6, 13
- [53] Yair Movshovitz-Attias, Alexander Toshev, Thomas K Leung, Sergey Ioffe, and Saurabh Singh. No fuss distance metric learning using proxies. In *CVPR*, pages 360–368, 2017. 3
- [54] Yuval Netzer, Tao Wang, Adam Coates, Alessandro Bissacco, Baolin Wu, Andrew Y Ng, et al. Reading digits in natural images with unsupervised feature learning. In *NIPS workshop on deep learning and unsupervised feature learning*, page 7. Granada, Spain, 2011. 13
- [55] Cuong V Nguyen, Alessandro Achille, Michael Lam, Tal Hassner, Vijay Mahadevan, and Stefano Soatto. Toward understanding catastrophic forgetting in continual learning. *arXiv preprint arXiv:1908.01091*, 2019. 1
- [56] M-E Nilsback and Andrew Zisserman. A visual vocabulary for flower classification. In *CVPR*, pages 1447–1454. IEEE, 2006. 13
- [57] Maria-Elena Nilsback and Andrew Zisserman. Automated flower classification over a large number of classes. In *ICVGIP*. IEEE, 2008. 12, 13
- [58] Omkar M Parkhi, Andrea Vedaldi, Andrew Zisserman, and CV Jawahar. Cats and dogs. In *CVPR*, pages 3498–3505. IEEE, 2012. 13
- [59] Yash Patel, Giorgos Tolias, and Jiří Matas. Recall@k surrogate loss with large batches and similarity mixup. In *CVPR*, pages 7502–7511, 2022. 3
- [60] Wenjie Pei, Tongqi Xia, Fanglin Chen, Jinsong Li, Jiandong Tian, and Guangming Lu. Sa²vp: Spatially aligned-and-adapted visual prompt. In *AAAI*, 2024. 2
- [61] Jonas Pfeiffer, Andreas Rücklé, Clifton Poth, Aishwarya Kamath, Ivan Vulić, Sebastian Ruder, Kyunghyun Cho, and Iryna Gurevych. Adapterhub: A framework for adapting transformers. *arXiv preprint arXiv:2007.07779*, 2020. 1
- [62] Alec Radford, Jong Wook Kim, Chris Hallacy, Aditya Ramesh, Gabriel Goh, Sandhini Agarwal, Girish Sastry, Amanda Askell, Pamela Mishkin, Jack Clark, et al. Learning transferable visual models from natural language supervision. In *ICML*, pages 8748–8763. PMLR, 2021. 2
- [63] Alec Radford, Jong Wook Kim, Chris Hallacy, Aditya Ramesh, Gabriel Goh, Sandhini Agarwal, Girish Sastry, Amanda Askell, Pamela Mishkin, Jack Clark, et al. Learning transferable visual models from natural language supervision. In *ICML*, pages 8748–8763. PMLR, 2021. 1

- [64] Li Ren, Kai Li, LiQiang Wang, and Kien Hua. Beyond the deep metric learning: enhance the cross-modal matching with adversarial discriminative domain regularization. In *ICPR*, pages 10165–10172. IEEE, 2021. 3
- [65] Li Ren, Chen Chen, Liqiang Wang, and Kien Hua. Towards improved proxy-based deep metric learning via data-augmented domain adaptation. In *AAAI*, 2024. 3
- [66] Li Ren, Chen Chen, Liqiang Wang, and Kien A. Hua. Learning semantic proxies from visual prompts for parameter-efficient fine-tuning in deep metric learning. In *ICLR*, 2024. 1, 3
- [67] Karsten Roth, Oriol Vinyals, and Zeynep Akata. Non-isotropy regularization for proxy-based deep metric learning. In *CVPR*, pages 7420–7430, 2022. 3
- [68] Sam Roweis, Geoffrey Hinton, and Ruslan Salakhutdinov. Neighbourhood component analysis. *NeurIPS*, 2004. 3
- [69] Chen Sun, Abhinav Shrivastava, Saurabh Singh, and Abhinav Gupta. Revisiting unreasonable effectiveness of data in deep learning era. In *ICCV*, pages 843–852, 2017. 1
- [70] Eu Wern Teh, Terrance DeVries, and Graham W Taylor. Proxynca++: Revisiting and revitalizing proxy neighborhood component analysis. In *ECCV*, pages 448–464. Springer, 2020. 3, 5
- [71] Hugo Touvron, Louis Martin, Kevin Stone, Peter Albert, Amjad Almahairi, Yasmine Babaei, Nikolay Bashlykov, Soumya Batra, Prajjwal Bhargava, Shriti Bhosale, et al. Llama 2: Open foundation and fine-tuned chat models. *arXiv preprint arXiv:2307.09288*, 2023. 2
- [72] Yun-Yun Tsai, Chengzhi Mao, and Junfeng Yang. Convolutional visual prompt for robust visual perception. *Advances in Neural Information Processing Systems*, 36, 2024. 3
- [73] Cheng-Hao Tu, Zheda Mai, and Wei-Lun Chao. Visual query tuning: Towards effective usage of intermediate representations for parameter and memory efficient transfer learning. In *CVPR*, pages 7725–7735, 2023. 2
- [74] Grant Van Horn, Steve Branson, Ryan Farrell, Scott Haber, Jessie Barry, Panos Ipeirotis, Pietro Perona, and Serge Belongie. Building a bird recognition app and large scale dataset with citizen scientists: The fine print in fine-grained dataset collection. In *CVPR*, pages 595–604, 2015. 12, 13
- [75] Ashish Vaswani, Noam Shazeer, Niki Parmar, Jakob Uszkoreit, Llion Jones, Aidan N Gomez, Łukasz Kaiser, and Illia Polosukhin. Attention is all you need. *NeurIPS*, 30, 2017. 2
- [76] Ashish Vaswani, Noam Shazeer, Niki Parmar, Jakob Uszkoreit, Llion Jones, Aidan N Gomez, Łukasz Kaiser, and Illia Polosukhin. Attention is all you need. *Neurips*, 30, 2017. 3
- [77] Bastiaan S Veeling, Jasper Linmans, Jim Winkens, Taco Cohen, and Max Welling. Rotation equivariant cnns for digital pathology. In *MICCAI*, pages 210–218. Springer, 2018. 13
- [78] Shashanka Venkataramanan, Bill Psomas, Yannis Avrithis, Ewa Kijak, Laurent Amsaleg, and Konstantinos Karantzas. It takes two to tango: Mixup for deep metric learning. *ICLR*, 2022. 3
- [79] Catherine Wah, Steve Branson, Peter Welinder, Pietro Perona, and Serge Belongie. The caltech-ucsd birds-200-2011 dataset. 2011. 12, 13
- [80] Bokun Wang, Yang Yang, Xing Xu, Alan Hanjalic, and Heng Tao Shen. Adversarial cross-modal retrieval. In *Multi-media*, pages 154–162, 2017. 3
- [81] Yaoming Wang, Bowen Shi, Xiaopeng Zhang, Jin Li, Yuchen Liu, Wenrui Dai, Chenglin Li, Hongkai Xiong, and Qi Tian. Adapting shortcut with normalizing flow: An efficient tuning framework for visual recognition. In *CVPR*. IEEE, 2023. 7
- [82] Yuzhu Wang, Lechao Cheng, Chaowei Fang, Dingwen Zhang, Manni Duan, and Meng Wang. Revisiting the power of prompt for visual tuning. *arXiv preprint arXiv:2402.02382*, 2024. 2, 8, 14
- [83] Jianxiong Xiao, James Hays, Krista A Ehinger, Aude Oliva, and Antonio Torralba. Sun database: Large-scale scene recognition from abbey to zoo. In *CVPR*, pages 3485–3492. IEEE, 2010. 13
- [84] Enze Xie, Lewei Yao, Han Shi, Zhili Liu, Daquan Zhou, Zhaoqiang Liu, Jiawei Li, and Zhenguo Li. Diffit: Unlocking transferability of large diffusion models via simple parameter-efficient fine-tuning. In *CVPR*, pages 4230–4239, 2023. 2
- [85] Seungryong Yoo, Eunji Kim, Dahuin Jung, Jungbeom Lee, and Sungroh Yoon. Improving visual prompt tuning for self-supervised vision transformers. In *ICML*, pages 40075–40092. PMLR, 2023. 2, 7, 14
- [86] Elad Ben Zaken, Shauli Ravfogel, and Yoav Goldberg. Bitfit: Simple parameter-efficient fine-tuning for transformer-based masked language-models. *arXiv preprint arXiv:2106.10199*, 2021. 1, 2, 5, 7, 17
- [87] Xiaohua Zhai, Joan Puigcerver, Alexander Kolesnikov, Pierre Ruyssen, Carlos Riquelme, Mario Lucic, Josip Djolonga, Andre Susano Pinto, Maxim Neumann, Alexey Dosovitskiy, et al. A large-scale study of representation learning with the visual task adaptation benchmark. *arXiv preprint arXiv:1910.04867*, 2019. 2, 6, 12, 13
- [88] Qizhe Zhang, Bocheng Zou, Ruichuan An, Jiaming Liu, and Shanghang Zhang. Mosa: Mixture of sparse adapters for visual efficient tuning. *arXiv preprint arXiv:2312.02923*, 2024. 7
- [89] Yuanhan Zhang, Kaiyang Zhou, and Ziwei Liu. Neural prompt search. *arXiv preprint arXiv:2206.04673*, 2022. 2
- [90] Sixiao Zheng, Jiachen Lu, Hengshuang Zhao, Xiatian Zhu, Zekun Luo, Yabiao Wang, Yanwei Fu, Jianfeng Feng, Tao Xiang, Philip HS Torr, et al. Rethinking semantic segmentation from a sequence-to-sequence perspective with transformers. In *CVPR*, pages 6881–6890, 2021. 12
- [91] Bolei Zhou, Hang Zhao, Xavier Puig, Tete Xiao, Sanja Fidler, Adela Barriuso, and Antonio Torralba. Semantic understanding of scenes through the ade20k dataset. *IJCV*, 127:302–321, 2019. 6, 13

Appendix

A. Details About the Experiments

A.1. Datasets

Classification Datasets. FGVC encompasses five fine-grained visual classification datasets: CUB-200-2011 [79], NABirds [74], Oxford Flowers [57], Stanford Dogs [35], and Stanford Cars [21]. Following Jia et al. [33], we split each dataset into `train` (90%) and `val` (10%) subsets.

VTAB-1K contains 19 diverse visual tasks across three categories: (i) *Natural* tasks involving standard camera images for object classification and scene recognition; (ii) *Specialized* tasks using domain-specific imagery such as medical scans and satellite data; and (iii) *Structured* tasks focusing on spatial relationships and object properties.

Segmentation Datasets. We evaluate on two semantic segmentation benchmarks: **ADE20K** with 150 fine-grained semantic concepts, and **PASCAL Context** providing pixel-wise annotations across 60 object classes. For dataset partitioning, we strictly follow the protocol established in VPT [33]. Complete dataset statistics and task details are provided in Table 6.

A.2. Implementation Details

Classification Tasks. For FGVC datasets, we employ standard data augmentation: random resizing and cropping to 224×224 pixels with random horizontal flipping. For VTAB-1K, following Zhai et al. [87] and Jia et al. [33], images are directly resized to 224×224 pixels without additional augmentation.

Model training utilizes the AdamW optimizer with a batch size of 32 over 100 epochs. The learning rate follows a combined schedule: a 10-epoch linear warm-up followed by cosine decay [48] from the initial value to $1e-8$. We determine optimal hyperparameters through cross-validation on the validation set. Following established protocols [19, 33, 45], we report mean accuracy across three runs with different random seeds.

Segmentation Tasks. We implement our experiments using the SETR framework [90] through MMSegmentation. We adopt the SETR-PUP configuration, utilizing one primary head and three auxiliary heads to process features from transformer layers 9, 12, 18, and 24. Training follows Zheng et al. [90]: 160k iterations for ADE20K and 80k iterations for PASCAL Context, with hyperparameter optimization mirroring our classification approach.

For multi-class segmentation samples, we adapt the class assignment strategy by randomly selecting one non-background class as the target class for visual prompt assign-

ment during each iteration, accounting for the pixel-wise multi-class nature of segmentation tasks.

A.3. Hyperparameter Configuration

Parameter Search Space. Table 5 details our hyperparameter search space for each task, including learning rate, weight decay, and the number and location of layers guided by semantic metrics loss. For the main results, we maintain default values for Proxy-Anchor loss parameters to narrow the parameter searching space.

Configuration	Value
Optimizer	AdamW [49]
Base learning rate range	{ $1e-3$, $5e-4$, $1e-4$, $5e-5$ }
Weight decay range	{0.001, 0.005, 0.01, 0.05, 0.1, 0.5, 1.0}
Learning rate schedule	Cosine Decay [48]
Layers applied guidance	{ 12, 10, 8, 6, 4, 2, 0 }
Num of prompts applied guidance	{ 5, 10, 20, 40 }
Proxy-Anchor δ	32.0
Proxy-Anchor τ	10.0
Batch size	32
Warmup epoch	10
Total epoch	100 (ViT-B/16)
Augmentation	RandomResizedCrop, RandomHorizontalFlip

Table 5. Hyper Parameters Searching Space and Training configuration in our experiments

Prompt Configuration for Tasks with Limited Classes.

For tasks with limited classes ($C < 5$), we augment the visual prompts by adding extra unassigned prompts that are not guided by semantic metrics loss. This approach empirically improves prompt transferability, particularly in tasks with very few classes (e.g., Patch Camelyon, Retinopathy, or KITTI-Dist in VTAB). The extra prompts help maintain an effective number of visual prompts in the guiding layer while preserving the semantic structure of the original class-assigned prompts.

B. Discussion and Comparison with Self-SPT

Methodological Distinctions. While both Self-SPT and our work leverage prompt distributions to enhance representation learning, they differ fundamentally in their approaches. Self-SPT attempts to align prompt and visual token distributions through initialization, using mean or max pooling of input data to set background values. In contrast, our method achieves distribution matching at the semantic level throughout the optimization process. This semantic-level matching enables our visual prompts to capture discriminative features by explicitly considering class relationships during training.

Our Key Advantages. Our approach demonstrates several significant advantages over Self-SPT:

- **Continuous Optimization:** Our method maintains distribution regularization throughout the entire optimization

Datasets	Task Description	Classes	Train Size	Val Size	Test Size
Fine-Grained Visual Classification (FGVC) [33]					
CUB-200-2011 [79]	Fine-grained Bird Species Recognition	200	5,394	600	5,794
NABirds [74]	Fine-grained Bird Species Recognition	55	21,536	2,393	24,633
Oxford Flowers [57]	Fine-Grained Flower Species recognition	102	1,020	1,020	6,149
Stanford Dogs [35]	Fine-grained Dog Species Recognition	120	10,800	1,200	8,580
Stanford Cars [21]	Fine-grained Car Classification	196	7,329	815	8,041
Visual Task Adaptation Benchmark (VTAB-1k) [87]					
Caltech101 [17]	Natural-Tasks (7) Natural images captured using standard cameras.	102	800/1000	200	6,084
CIFAR-100 [40]		100			10,000
DTD [9]		47			1,880
Oxford-Flowers102 [56]		102			6,149
Oxford-PetS [58]		37			3,669
SVHN [54]		10			26,032
Sun397 [83]		397			21,750
Patch Camelyon [77]	Special-Tasks (4) Images captured via specialized equipments	2	800/1000	200	32,768
EuroSAT [29]		10			5,400
Resisc45 [7]		45			1,880
Retinopathy [15]		5			42,670
Clevr/count [34]	Structured-Tasks (8) Require geometric comprehension	6	800/1000	200	15,000
Clevr/distance [34]		6			15,000
DMLab [1]		6			22,735
KITTI-Dist [22]		4			711
dSprites/location [51]		16			73,728
dSprites/orientation [51]		16			73,728
SmallNORB/azimuth [42]		18			12,150
SmallNORB/elevation [42]		18			12,150
Image Semantic Segmentation					
ADE20K [91]	Fine-grained images with pixel-wise semantic annotations	150	20210	2000	3352
PASCAL Context [52]		60	4998	5105	—

Table 6. The details and specifications of the downstream task datasets we selected to evaluate our proposed framework.

process, while Self-SPT only applies distribution alignment during initialization.

- **Discriminative Feature Learning:** Through metric guidance, our prompts explicitly capture class-specific discriminative features by comparing tokens from the same and different classes. In contrast, Self-SPT’s uniform background value initialization does not differentiate between class-specific features.
- **Computational Efficiency:** Our method significantly reduces pre-processing overhead by clustering class representations rather than entire visual token sets, avoiding the computational burden of Self-SPT’s k-means clustering approach on the full dataset.

Empirical Analysis. To thoroughly evaluate the relationship between background value initialization and metric guidance learning, we attempted to reproduce Self-SPT’s results and assess its performance when integrated with our method. As illustrated in Figure 5, our experiments revealed two key findings: (1) we were unable to reproduce the performance metrics reported in the original Self-SPT paper,

and (2) the background value initialization strategy did not yield measurable improvements when combined with our metric guidance approach. These results further validate our focus on semantic-level distribution matching as the primary mechanism for improving prompt optimization.

The comparative analysis demonstrates that while both methods address prompt distribution optimization, our approach offers *more robust theoretical foundations, better computational efficiency, and superior empirical performance*. The continuous nature of our distribution regularization, combined with explicit semantic guidance, provides a more principled framework for learning discriminative prompt representations.

C. DA-VPT+: Integration with Bias Tuning

This section examines the synergy between our proposed metric learning guidance and bias tuning in PEFT models. Our investigation is motivated by an intriguing observation from the original VPT work [33], which reported that bias tuning adversely affects vanilla VPT optimization. We present a novel perspective on this interaction and demon-

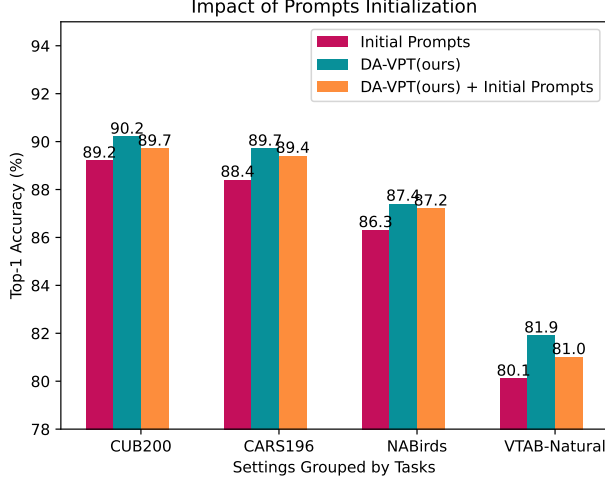


Figure 5. **Impact of Prompt Initialization Strategies.** Comparative analysis of model performance under different prompt initialization schemes. Results demonstrate that the background value initialization method proposed in Self-SPT [82], which uses mean pooled visual tokens, shows no significant performance gains when combined with our distribution-aware guidance approach. This suggests that our method’s effectiveness stems from its continuous distribution matching during training rather than initial prompt configurations.

strate how our approach effectively addresses these limitations.

Theoretical Motivation. The distribution of visual tokens in transformer layers is inherently constrained by the representations from previous layers and their associated visual prompts. We hypothesize that unfreezing bias terms, particularly in Key and Value projections, introduces additional flexibility in token representation. This flexibility becomes especially significant when combined with our metric learning guidance, as it allows for more nuanced distribution alignment between visual prompts and tokens.

Advantages over Vanilla VPT. Unlike vanilla VPT, DA-VPT explicitly manages distribution alignment between visual prompts and tokens through metric learning guidance. This explicit alignment makes our method more responsive to distribution shifts in visual tokens, which are substantially influenced by projection layer bias terms. By simultaneously optimizing bias terms and maintaining distribution alignment, DA-VPT+ achieves more robust and effective feature representations. This integration of bias tuning with DA-VPT demonstrates how our method’s distribution-aware approach can transform a previously problematic component (bias tuning) into a complementary enhancement.

Methods	CUB200	Cars	NABirds	VTAB-Natural
VPT (baseline)	88.6	87.4	85.7	78.48
DA-VPT	90.2 (+1.6)	89.7 (+2.3)	87.4 (+1.7)	80.25 (+1.77)
DA-VPT+Conn	89.6 (+1.0)	88.1 (+0.7)	86.8 (+1.1)	79.11 (+0.63)
DA-VPT+Gate	89.8 (+1.2)	88.4 (+1.0)	87.0 (+1.3)	79.48 (+1.00)
DA-VPT (PNCA)	89.2 (+0.6)	88.2 (+0.8)	86.9 (+1.2)	79.22 (+0.74)
DA-VPT (triplet)	87.9 (-0.7)	87.1 (-0.3)	85.4 (-0.3)	78.61 (+0.13)

Table 7. **Analysis of Connection Structures and Metric Learning Variants.** Empirical evaluation of (a) different visual prompt connection architectures across transformer layers and (b) alternative metric learning approaches. Our results indicate that neither cross-layer connections nor learnable activation gates provide substantial improvements over our base method. Furthermore, experiments with alternative metric learning losses show less stable fine-tuning performance compared to our approach, with some variants performing below the VPT baseline. These findings suggest that the effectiveness of our method primarily stems from its distribution-aware prompt optimization rather than architectural modifications or alternative metric formulations.

D. Supplemental Empirical Studies

We conduct additional empirical investigations to explore potential extensions of our proposed framework in two key directions: alternative metric learning approaches and modified architectural connections.

Alternative Metric Learning Losses. We investigate the effectiveness of different metric learning losses for guiding visual prompt distributions. Specifically, we compare our proposed Proxy-Anchor (PA) loss against two alternatives: vanilla Proxy-NCA loss and triplet loss. For these vanilla losses, we treat the selected prompts as individual data points, with class assignments determined by the current training epoch. This comparison helps us understand the relative advantages of our PA loss formulation in the context of prompt optimization. Details are listed in Table 7.

Modified Connection Structures. We examine two architectural modifications to the base framework: 1) Cross-layer prompt connections (DA-VPT+Conn), which enable information flow between prompts at different layers, and 2) Learnable gated connections following GateVPT [85] (DA-VPT+Gate), which introduce adaptive control over prompt interactions.

These architectural studies provide insights into the role of prompt connectivity in our distribution-aware framework. The experimental results and detailed analysis of these variations are presented in Table 7.

E. The Proof and Detail of theorem 1

Theorem 2. For a weight perturbation Δa_i calculated using the softmax function, there is an approximate relationship:

$$\Delta a_i \approx a_i(1 - a_i)\Delta s_i,$$

Algorithm 1 Distribution Aware Visual Prompt Tuning (DA-VPT)

Input: Pre-trained ViT model f_θ , Dataset $\mathcal{D} = (x_i, y_i)_{i=1}^N$, number of prompts M , β , λ , learning rate and other related hyperparameters

Output: Fine-tuned ViT model f_θ

Initialize M prompts \mathbf{p}^l for each layer l

Get class tokens $\mathbf{S} \in \mathbb{R}^{C \times D}$ by Forward passing f_θ

Create a mapping from C classes to M prompts ($C \rightarrow M$) using k-means clustering on \mathbf{S}

while stop criteria is not satisfied **do**

 Obtain a batch $\{x_i, y_i\}_{i=1}^n$ from \mathcal{D}

 Forward pass \mathbf{x}_i through ViT f_θ with prompts \mathbf{p}^l

 Select saliency patch \mathbf{x} right after attention layer in last selected blocks

 Calculate metric learning losses $\mathcal{L}_{\text{ML}}(\mathbf{x}, \mathbf{p})$ and $\mathcal{L}_{\text{ML}}(\mathbf{p}, \mathbf{x}_{\text{cls}})$

 Calculate cross-entropy loss \mathcal{L}_{CE}

 Minimize loss: $\mathcal{L} = \mathcal{L}_{\text{CE}} + \beta \mathcal{L}_{\text{ML}}(\mathbf{x}, \mathbf{p}) + \lambda \mathcal{L}_{\text{ML}}(\mathbf{p}, \mathbf{x}_{\text{cls}})$

 Update \mathbf{p} and other learnable parameters from Backward of \mathcal{L}

 Update class tokens \mathbf{S} and class-prompt mapping $C \rightarrow M$ after certain steps

return Fine-tuned ViT model f_θ

where Δs_i is a small change in the attention score s_i , and

$$\Delta s_i = \frac{\Delta p^\top v_i}{\sqrt{d}}.$$

Proof. The attention weights a_i are calculated using the softmax function applied to the attention scores s_i :

$$a_i = \frac{e^{s_i}}{\sum_j e^{s_j}}.$$

The partial derivative of a_i with respect to s_j is given by:

$$\frac{\partial a_i}{\partial s_j} = a_i(\delta_{ij} - a_j),$$

where δ_{ij} is the Kronecker delta function:

$$\delta_{ij} = \begin{cases} 1, & \text{if } i = j, \\ 0, & \text{if } i \neq j. \end{cases}$$

For small perturbations Δs_j , we can approximate the change in a_i using a first-order Taylor expansion:

$$\Delta a_i \approx \sum_j \frac{\partial a_i}{\partial s_j} \Delta s_j.$$

Then we substitute the expression for the derivative:

$$\Delta a_i \approx \sum_j a_i(\delta_{ij} - a_j) \Delta s_j.$$

Split the summation into two parts:

$$\Delta a_i \approx a_i(1 - a_i) \Delta s_i - a_i \sum_{j \neq i} a_j \Delta s_j.$$

We assume that the weighted sum of the perturbations Δs_j for $j \neq i$ is negligible:

$$\sum_{j \neq i} a_j \Delta s_j \approx 0.$$

This approximation is reasonable when:

- The perturbations Δs_j for $j \neq i$ are small and uncorrelated, so they average out.
- The attention weights a_j for $j \neq i$ are small (i.e., a_i is dominant).

Under this assumption, the expression simplifies to:

$$\Delta a_i \approx a_i(1 - a_i) \Delta s_i.$$

□

F. Limitations

Our Parameter-Efficient Fine-Tuning (PEFT) approach, while effective, still faces a few key challenges.

Hyperparameter Sensitivity. The introduction of metric learning losses alongside the standard cross-entropy loss creates additional complexity in hyperparameter optimization. The performance of our method depends significantly on the weight ratios β and λ , which require careful tuning for each combination of backbone model and downstream task. This dependency can make the optimization process more time-intensive compared to simpler PEFT approaches.

Computational Overhead. Our method introduces additional computational costs through the metric learning losses and their associated operations. While the increased latency remains within practical bounds (typically 5% higher than baseline PEFT methods), it may impact applications with strict real-time requirements or resource constraints.

Limited on some rare scenes Our proposed method is proper for tasks that have a comparable number of classes. In some special tasks that have a limited number of classes (e.g., Patch Camelyon, Retinopathy, or KITTI-Dist in VTAB-1k), the number of prompts should be the same as the classes that are too few to have enough transfer capacities. In this case, we suggest adding a few supplemental visual prompts

that are not assigned to class labels and are guided by the metric learning loss. In other words, we still propose to add normal visual prompts in addition to the guided prompts when the number of classes is very limited.

G. Future Works

To address these limitations, we plan to develop automated hyperparameter optimization strategies, potentially leveraging meta-learning or Bayesian optimization techniques. We will also investigate more efficient metric learning formulations that maintain performance while reducing computational overhead. Additionally, our research will explore hardware-specific optimizations to minimize the latency impact in practical deployments.

Despite these challenges, our experimental results demonstrate that the performance improvements offered by our method consistently outweigh its limitations across diverse tasks and model architectures.

H. Broader Impact

Distribution Aware Visual Prompt Tuning (DA-VPT) has significant implications for both technical advancement and societal applications.

Technical Contributions. Our method advances the performance in parameter-efficient fine-tuning by enabling more efficient adaptation of large vision models to specific domains. The reduced computational requirements for model specialization, coupled with improved performance on fine-grained visual tasks, make sophisticated vision models more accessible and practical for real-world applications.

Potential Applications. DA-VPT could enable significant advances in several high-impact domains. In healthcare, it can facilitate more accurate medical image analysis with limited training data, potentially improving diagnostic accuracy and treatment planning. Environmental protection efforts could benefit from enhanced wildlife monitoring and biodiversity assessment capabilities. The method’s efficiency also enables deployment of sophisticated vision models on edge devices, advancing assistive technologies for accessibility applications. Furthermore, industrial applications such as quality control and visual inspection systems could see substantial improvements in accuracy and reliability.

I. More Examples of Attention Maps on Prompts

We also demonstrate some representative attention visualizations from CUB-200-2011 and Stanford Dogs datasets. For each image, we display the attention map corresponding

Table 8. Summary of notation used throughout the paper.

Symbol	Domain	Description
\mathbf{I}	$\mathbb{R}^{H \times W \times C}$	Input image
N	\mathbb{N}	Number of image patches
D	\mathbb{N}	Dimension of embedding space
L	\mathbb{N}	Number of Transformer layers
l	$\{1, \dots, L\}$	Layer index
\mathbf{x}_{cls}	\mathbb{R}^D	Class [CLS] token
\mathbf{X}	$\mathbb{R}^{(N+1) \times D}$	Sequence of embeddings
\mathbf{H}_i	$\mathbb{R}^{D \times D}$	Attention head i
$\mathbf{Q}, \mathbf{K}, \mathbf{V}$	$\mathbb{R}^{N \times D}$	Query, Key, Value matrices
M	\mathbb{N}	Number of prompt tokens
\mathbf{P}	$\mathbb{R}^{M \times D}$	Set of prompt tokens
\mathbf{p}_k	\mathbb{R}^D	k -th prompt token
$\hat{\mathbf{x}}$	\mathbb{R}^D	L2-normalized vector of \mathbf{x}
y_i	$\{1, \dots, C\}$	Class label for sample i
C	\mathbb{N}	Number of classes
δ	\mathbb{R}^+	Margin in metric learning
τ	\mathbb{R}^+	Temperature parameter
\mathcal{P}	-	Set of all prompts
\mathcal{P}^+	-	Set of positive prompts
\mathcal{X}_p^+	-	Set of positive visual tokens
\mathcal{X}_p^-	-	Set of negative visual tokens
β, λ	\mathbb{R}^+	Loss weighting hyperparameters
\mathbf{S}	$\mathbb{R}^{C \times D}$	Class representations
\mathbf{W}_Q^l	$\mathbb{R}^{D \times D}$	Query projection matrix at layer l
$\mathbf{b}_K, \mathbf{b}_V$	\mathbb{R}^D	Bias terms for Key and Value projections

to its class-assigned prompt. The attention patterns demonstrate how our method learns to focus on class-discriminative regions.

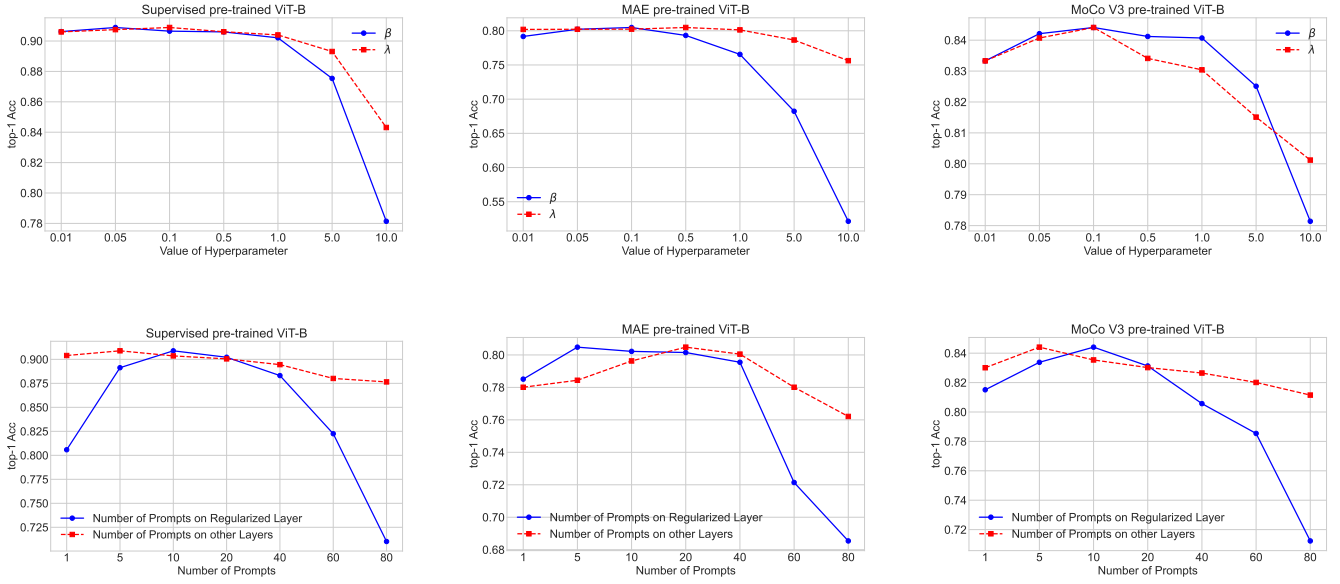


Figure 6. **Impact of Hyperparameters in Three Pre-trained Models on CUB-200-2011:** This figure illustrates the impact of hyperparameters on the performance of our proposed method across three pre-trained models (Supervised ViT, MAE, and MoCo-v3) on the CUB-200-2011 dataset. The hyperparameters investigated include the weight factors β and λ for the two proposed \mathcal{L}_{ML} losses, the number of prompts in the metric guidance layer, and the number of prompts in other layers. The results show that the optimal weight factors are less than 1.0, indicating that a balanced contribution from the \mathcal{L}_{ML} losses is beneficial for performance. Furthermore, the number of prompts in the guidance layer exhibits higher sensitivity compared to the number of prompts in other layers, suggesting that the choice of prompt configuration in the guidance layer plays a crucial role in the effectiveness of our method. These findings provide insights into the importance of carefully tuning the hyperparameters to achieve optimal performance across different pre-trained models.

Methods	Natural (7)							Specialized (4)				Structured (8)							
	CIFAR-100	Caltech101	DTD	Flowers102	Pets	SVHN	Sun397	Patch Camelyon	EuroSAT	Resisc45	Retinopathy	Clevr/count	Clevr/distance	DMLab	KITTI/distance	dSprites/loc	dSprites/ori	SmallNORB/azi	SmallNORB/ele
<i>ViT-B with supervised pre-trained on ImageNet-21K</i>																			
Full fine-tuning [33]	68.9	87.7	64.3	97.2	86.9	87.4	38.8	79.7	93.7	84.2	73.9	56.3	58.6	41.7	65.5	57.5	46.7	25.7	29.1
Linear probing [33]	63.4	85.0	63.2	97.0	86.3	36.6	51.0	78.5	87.5	68.6	74.0	34.3	30.6	33.2	55.4	12.5	20.0	9.6	19.2
Adapter [31]	74.1	86.1	63.2	97.7	87.0	34.6	50.8	76.3	88.0	73.1	70.5	45.7	37.4	31.2	53.2	30.3	25.4	13.8	22.1
Bias [86]	72.8	87.0	59.2	97.5	85.3	59.9	51.4	78.7	91.6	72.9	69.8	61.5	55.6	32.4	55.9	66.6	40.0	15.7	25.1
VPT-Deep [33]	78.8	90.8	65.8	98.0	88.3	78.1	49.6	81.8	96.1	83.4	68.4	68.5	60.0	46.5	72.8	73.6	47.9	32.9	37.8
DA-VPT+ (ours)	74.4	92.7	74.3	99.4	91.3	91.5	86.2	96.2	87.2	87.2	76.3	81.3	62.58	52.82	65.3	84.9	51	33.11	48.7
<i>ViT-B with MAE pre-trained on ImageNet-1K</i>																			
Full fine-tuning [33]	24.6	84.2	56.9	72.7	74.4	86.6	15.8	81.8	94.0	72.3	70.6	67.0	59.8	45.2	75.3	72.5	47.5	30.2	33.0
DA-VPT+ (ours)	38.7	87.6	64.6	83.5	86.1	83.6	22	85	94.6	79.0	73.2	77.6	63.8	46.9	65.7	90.8	53.0	28.8	47.7
<i>ViT-B with MoCo-V3 pre-trained on ImageNet-1K</i>																			
Full fine-tuning [33]	57.6	91.0	64.6	91.6	79.9	89.8	29.1	85.1	96.4	83.1	74.2	55.2	56.9	44.6	77.9	63.8	49.0	31.5	36.9
DA-VPT+ (ours)	63.5	90.7	69.8	92.5	90.6	90.5	40.5	85.8	96.0	83.9	73.2	80.5	62.3	49.8	63.7	84.2	52.2	30.3	48.9

Table 9. Results of details of performance comparisons on the VTAB-1k benchmark with ViT-B/16 models with supervised, MAE and MoCo-V3 pre-training.

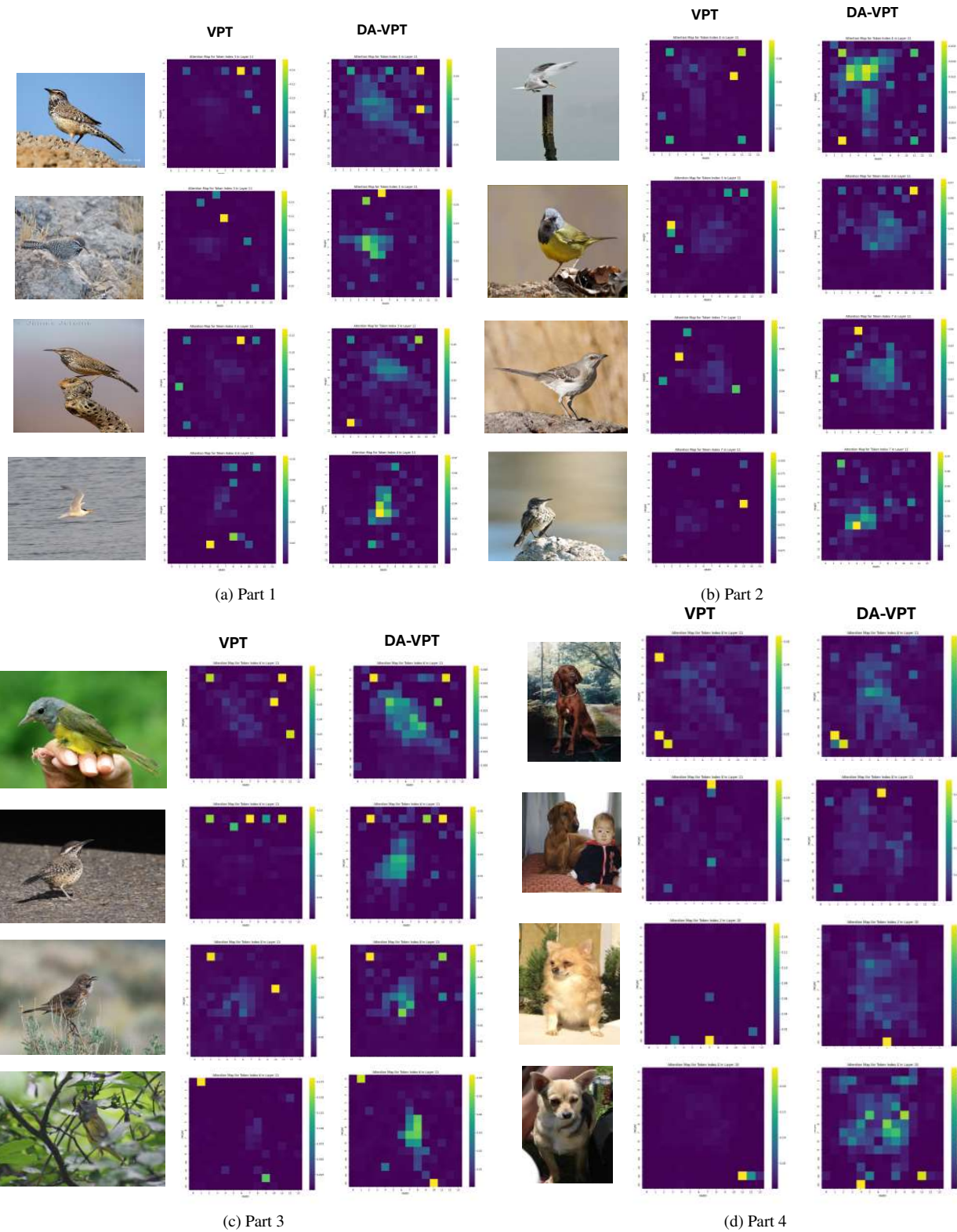


Figure 7. **Visualization of Class-Specific Attention Maps.** 7a,7b,7c: Examples from CUB-200-2011 showing fine-grained bird features. 7d: Examples from Stanford Dogs highlighting breed-specific characteristics. These visualizations illustrate the model’s ability to capture class-relevant visual features across different fine-grained classification tasks.